EJNMMI Research

ORIGINAL RESEARCH

Open Access

Optimal imaging time points considering accuracy and precision of Patlak linearization for ^{89}Zr-immuno-PET: a simulation study

Jessica E. Wijngaarden[1,4*], Marc C. Huisman[1,4], Johanna E. E. Pouw[2,4], C. Willemien Menke-van der Houven van Oordt[2,4], Yvonne W. S. Jauw[1,3,4] and Ronald Boellaard[1,4]

Abstract

Purpose: Zirconium-89-immuno-positron emission tomography (^{89}Zr-immuno-PET) has enabled visualization of zirconium-89 labelled monoclonal antibody (^{89}Zr-mAb) uptake in organs and tumors in vivo. Patlak linearization of ^{89}Zr-immuno-PET quantification data allows for separation of reversible and irreversible uptake, by combining multiple blood samples and PET images at different days. As one can obtain only a limited number of blood samples and scans per patient, choosing the optimal time points is important. Tissue activity concentration curves were simulated to evaluate the effect of imaging time points on Patlak results, considering different time points, input functions, noise levels and levels of reversible and irreversible uptake.

Methods: Based on ^{89}Zr-mAb input functions and reference values for reversible (V_T) and irreversible (K_i) uptake from literature, multiple tissue activity curves were simulated. Three different ^{89}Zr-mAb input functions, five time points between 24 and 192 h p.i., noise levels of 5, 10 and 15%, and three reference K_i and V_T values were considered. Simulated K_i and V_T were calculated (Patlak linearization) for a thousand repetitions. Accuracy and precision of Patlak linearization were evaluated by comparing simulated K_i and V_T with reference values.

Results: Simulations showed that K_i is always underestimated. Inclusion of time point 24 h p.i. reduced bias and variability in V_T, and slightly reduced bias and variability in K_i, as compared to combinations of three later time points. After inclusion of 24 h p.i., minimal differences were found in bias and variability between different combinations of later imaging time points, despite different input functions, noise levels and reference values.

Conclusion: Inclusion of a blood sample and PET scan at 24 h p.i. improves accuracy and precision of Patlak results for ^{89}Zr-immuno-PET; the exact timing of the two later time points is not critical.

Keywords: ^{89}Zr-immuno-PET, Patlak linearization, Monoclonal antibody, Molecular imaging

Introduction

Therapeutic monoclonal antibodies (mAbs) are used in cancer treatment both in targeted therapy and in immunotherapy [1]. mAbs directly elicit their effect on their target or indirectly through mediation by the immune system. The effectiveness of this therapy is, however, patient specific and the therapy can cause serious side effects. Gaining more insight into the mechanisms of mAbs by tracking them inside the body may improve cancer treatment with mAbs.

Zirconium-89-immuno-positron emission tomography (^{89}Zr-immuno-PET) allows visualization and quantification of the uptake of zirconium-89 labelled mAbs (^{89}Zr-mAbs) in tumors and organs in vivo. The relatively long half-life of ^{89}Zr is sufficient for imaging mAbs during

*Correspondence: j.e.wijngaarden@amsterdamumc.nl

[1] Department of Radiology and Nuclear Medicine, Amsterdam UMC location Vrije Universiteit Amsterdam, Boelelaan 1117, Amsterdam, The Netherlands
Full list of author information is available at the end of the article

the time they need to reach tissues [2]. Quantification of ^{89}Zr-mAb uptake is commonly done using the standardized uptake value (SUV). SUV is defined as the activity concentration in a volume of interest, divided by the injected activity per unit of body weight [3]. Since SUV is a single value obtained from a single PET scan, SUV is not able to distinguish between non-specific ^{89}Zr-mAb uptake in the blood or interstitial space volume fraction of the tissue, and specific uptake due to target engagement, unless either specific or non-specific uptake can be assumed to be negligible. In general, both non-specific and specific uptake contribute to the total uptake signal. Additionally, SUV considers only the injected activity and not the ^{89}Zr-mAb plasma clearance over time [4].

An approach that does consider plasma activity concentrations for analyzing PET images is the use of compartment models [5]. Using a two-tissue compartment model assuming irreversible uptake of tracer, Patlak linearization can be applied [6]. A two-tissue irreversible compartment model is applicable to ^{89}Zr-mAb uptake, because ^{89}Zr residualizes in the tissue after mAb catabolism or target engagement [2]. The uptake of ^{89}Zr-mAbs in tissue is quantified relative to the concentration of ^{89}Zr-mAbs in blood plasma over time and therefore requires multiple blood samples and PET images. Since ^{89}Zr-mAbs circulate in the body for several days [7], capturing the pharmacokinetics of ^{89}Zr-mAbs requires multiple sampling days. However, minimizing the number of scans and samples is important in terms of patient safety and comfort. Selecting the optimal time points for blood sampling and PET imaging of ^{89}Zr-mAbs is therefore crucial.

Patlak linearization provides several advantages over SUV. From Patlak linearization, reversible and irreversible ^{89}Zr-mAb uptake can be quantified per volume of interest. Additionally, Patlak can potentially also distinguish between non-specific and specific ^{89}Zr-mAb uptake, by comparing Patlak results to baseline Patlak values for tissues without target expression [8]. Moreover, Patlak linearization uses the measured plasma kinetics and thus takes variations in plasma clearance between subjects or at various mass doses into account. Yet, like SUV, Patlak linearization assumes that receptor availability or occupancy remains constant during the course of the PET studies and does not consider redistribution of cells or targets, as will be discussed later.

Previous research has applied Patlak linearization for quantifying ^{89}Zr-mAbs uptake in patients [8, 9]. In these studies, PET scans were obtained two to four times between 2 and 192 h p.i. Blood was sampled up to five times on the day of injection and with every PET scan [8, 9]. This resulted in a maximum of three time points for Patlak linearization. The unavoidable sparse data sampling introduces uncertainties in the data which may affect Patlak results. Evaluating the magnitude of the effects of sparse data sampling will provide more information on the accuracy and precision of Patlak results.

In this study, the effect of imaging time points on the accuracy and precision of Patlak results was evaluated by means of simulations, including the following variables: different input functions (IFs), different noise levels for tissue activity curves (TACs) and tissues with different levels of reversible and irreversible uptake.

Methods

To study the effects of different time points on Patlak results, TACs were simulated using Patlak linearization, three time points were included, noise was added and Patlak values were calculated. These steps were repeated as a function of different variables.

Patlak linearization

Patlak linearization can be used to estimate the irreversible and reversible uptake of ^{89}Zr-mAb in tissue based on graphical analysis of multiple-time tissue uptake data [6]. The analysis is based on a compartment model consisting of a reversible and an irreversible tissue compartment. The reversible tissue compartment represents ^{89}Zr-mAb in the plasma and interstitial space of the tissue or reversible target binding, and reaches an equilibrium state after some time. The irreversible tissue compartment represents irreversible binding of ^{89}Zr-mAb (e.g., non-specific catabolism or irreversible target binding). After equilibrium is reached, the activity concentration in tissue (AC_t) is the sum of both parts. The reversible part is then proportional to the activity concentration in plasma (AC_p) and the irreversible part is proportional to the area under the curve (AUC) of the AC_p (AUC_p), which is the integral of AC_p (Eq. 1). Dividing both sides of Eq. 1 by AC_p results in a linear relation known as the Patlak equation (Eq. 2) [6, 9]. The slope of this equation is K_i, which represents the nett rate of irreversible uptake [h^{-1}]. K_i is a measure for the catabolic rate of tissue without target expression and a measure for both catabolic rate and target engagement of tissue with target expression [8]. The offset is the V_T, the ratio between tissue and plasma concentration at equilibrium, which is related to the reversible part. (Eq. 2).

$$AC_t = K_i \cdot AUCp + V_T \cdot AC_p \tag{1}$$

$$\frac{AC_t}{AC_p} = K_i \cdot \frac{\int_0^t AC_P(x)dx}{AC_P} + V_T \tag{2}$$

Multiple population IFs were obtained from literature as input for the AC_p. A literature search for papers

containing plasma/serum sampling data of ^{89}Zr-mAb concentration in humans resulted in five papers as listed in Table 1. From these papers, the concentration ^{89}Zr labelled mAbs in plasma/serum over time was obtained using PlotDigitizer (version 2.6.8, http://plotdigitizer.sourceforge.net/). The purpose of using IFs from literature was to use IFs that could be obtained in practice. Therefore, instead of using the raw data points, a bi-exponent (Eq. 3) was fitted through the data, see Fig. 1. The concentrations of the three IFs ^{89}Zr-trastuzumab, ^{89}Zr-pertuzumab and ^{89}Zr-huJ591 were chosen as input for AC_p in the simulations, as they presented three different clearance rates.

The Patlak equation is used to simulate AC_t as function of AC_p, K_i and V_T, i.e., to generate TAC_s. The given K_i and V_T for generating the TAC are called 'reference K_i (rK_i)' and 'reference V_T (rV_T)'. The mathematical derivation for the TAC is as follows. AC_p is described by a bi-exponential function (Eq. 3). AUC_p can be obtained by integration of Eq. 3 between moment of injection and moment of PET scan, resulting in Eq. 4. Substitution of Eqs. 3 and 4 into Eq. 1 gives the equation for the TAC (AC_t) as a function of rK_i, rV_T and coefficients of the bi-exponential equation of the IF (Eq. 5):

$$AC_p = A \cdot e^{ax} + B \cdot e^{bx} \tag{3}$$

$$\begin{aligned} AUCp &= \int_0^t \left(A \cdot e^{ax} + B \cdot e^{bx}\right) dx \\ &= \frac{A \cdot \left(e^{ax} - 1\right)}{a} + \frac{B \cdot \left(e^{bx} - 1\right)}{b} \end{aligned} \tag{4}$$

Table 1 Five papers provided ^{89}Zr-mAb plasma/serum activity concentration data

	^{89}Zr-mAb	Subject group	Sampling	References
1	^{89}Zr-huJ591	Metastatic prostate cancer	Serum	Pandit-Taskar et al. [10]
2	^{89}Zr-trastuzumab	Esophagogastric cancer	Serum	O'Donoghue et al. [11]
3	^{89}Zr-pertuzumab	Breast cancer	Serum	Ulaner et al. [12]
4	^{89}Zr-DFO-MSTP2109A	Prostate cancer	Plasma	O'Donoghue et al. [13]
5	^{89}Zr-AlbudAb	Healthy volunteers	Plasma	Thorneloe et al. [14]

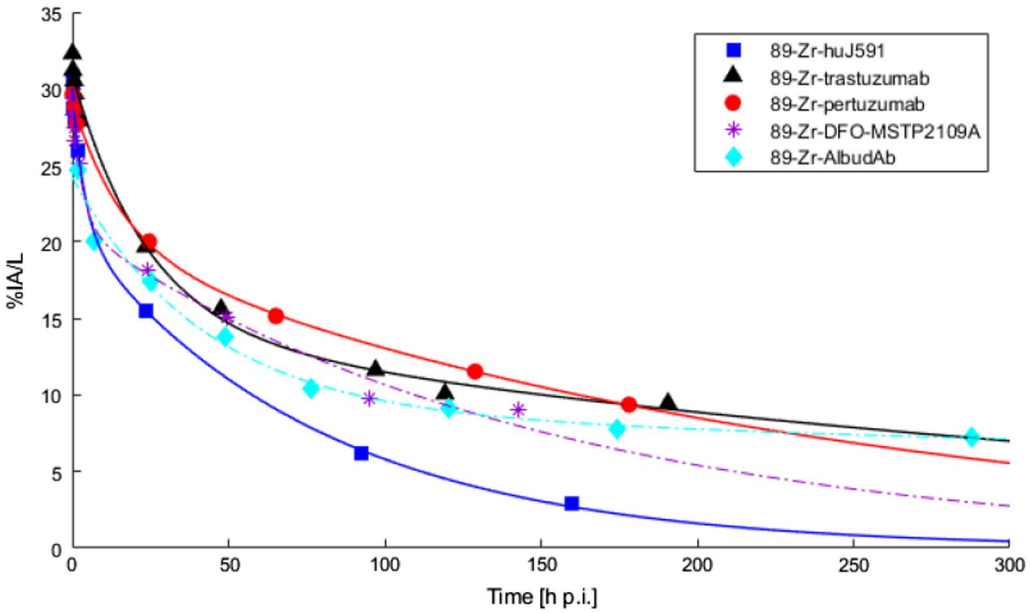

Fig.1 Plasma or serum activity concentrations in percentage injected activity per liter as a function of time in hours post-injection for ^{89}Zr-huJ591 (191.3 ± 9 MBq, 25 mg) [10], ^{89}Zr-trastuzumab (185 MBq, 50 mg) [11], ^{89}Zr-pertuzumab (74 MBq, 20 or 50 mg) [12], ^{89}Zr-DFO-MSTP2109A (184 MBq, 10 mg) [13] and ^{89}Zr-AlbudAb (14 MBq, 1 mg) [14]. The bold lines represent the input functions used for the simulations, and the dashed lines represent the input functions not included in the simulations. %IA/L = percentage injected activity per liter, h p.i. = hours post-injection

$$\mathrm{AC}_t = rK_i \cdot \left(\frac{A \cdot \left(\mathrm{e}^{ax} - 1\right)}{a} + \frac{B \cdot \left(\mathrm{e}^{bx} - 1\right)}{b} \right) + rV_t \cdot \left(A \cdot \mathrm{e}^{ax} + B \cdot \mathrm{e}^{bx} \right) \quad (5)$$

Sparse sampling and noise

For a given IF, rK_i and rV_T, values for AC_p and AC_t were determined with the equations above on three given time points, mimicking the sparse sampling in practice. AUC_p was determined, but now by numerical integration of the IF, considering only four time points of AC_p (see red line first panel Fig. 2). Additionally, noise was added to values for AC_t at the given three time points. Standard deviations (SDs) of AC_t were approximated based on counting statistics, which behaves as a Poisson distribution with SD≈√N and N is number of counts [15]. The SD at any given time point was approximated with Eq. 6, where the SD at $t=0$ is predefined. Assuming equal scanning durations within a study, the ratio N(0):N(t) is assumed to be equal to the ratio between non-decay corrected activity concentrations $\mathrm{ncAC}_t(0)$:ncAC_t(t) (Eq. 7). To incorporate variability in the standard deviation, noise was added using the MATLAB function randn [16]. Subsequently, the percentage SD was calculated and applied on the decay corrected AC_t for adding noise to AC_t (Eq. 8).

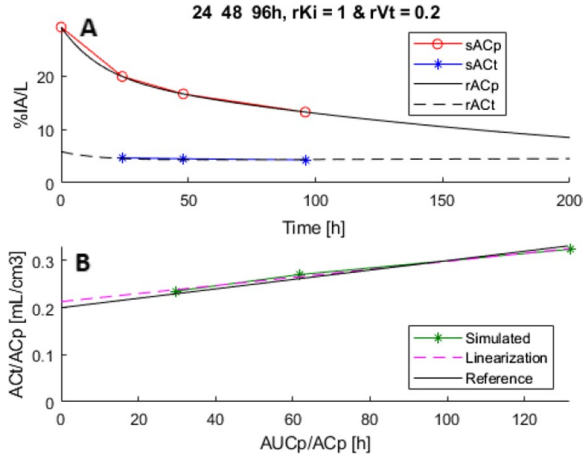

Fig. 2 Patlak linearization for ^{89}Zr-pertuzumab input function and time activity curves with 5% noise, $rK_i = 1 \cdot 10^{-3}$ [h^{-1}], $rV_T = 0.2$ and time points 24, 48 and 96 h post-injection. **A**: Activity concentrations in plasma (red) and tissue (blue), full curve based on reference values (rAC_p and rAC_t) and calculated based on simulations (sAC_p and sAC_t) in percentage injected activity per liter as a function of time p.i. **B**: Patlak plot; activity concentration in tissue (AC_t) divided by activity concentration in plasma (AC_p) as a function of area under the plasma curve (AUC_p) divided by activity concentration in plasma (AC_p). Based on reference values (black), simulated values (green) and linear regression of the simulated values (pink). %IA/L = percentage injected activity per liter

$$\mathrm{SD}(t) = \frac{\mathrm{SD}(0)}{\sqrt{N(0)/N(t)}} \quad (6)$$

$$\mathrm{SD}(t) = \frac{\mathrm{SD}(0)}{\sqrt{\mathrm{ncAC}_t(0)/\mathrm{ncAC}_t(t)}} \quad (7)$$

$$AC_{t,noise}(t) = AC_t(t) + AC_t(t) * \%SD(t) * randn \quad (8)$$

Variability in AC_p as a result of counting statistics ranged from SD = 0.2–0.4%, based on previously in house counted blood samples. The noise in AC_p was assumed to be negligible compared to the noise in the TAC and was not included in the simulations.

Patlak analysis of simulated TACs

Subsequently, Patlak linearization (Eq. 2) was applied on the generated AC_p, AUC_p and AC_t with noise on the given time points, from which the slope (K_i) and offset (V_T) could be determined, see Fig. 2. Simulations were repeated 1000 times to incorporate the effect of noise. The mean and standard error (SE) of the simulated K_i and V_T were obtained to compare with rK_i and rV_T for evaluating bias and variability.

Performance of Patlak analysis

Accuracy and precision of Patlak results were evaluated as a function of the following variables: time points of evaluation, rK_i and rV_T, and noise level of AC_t. Each simulation included a time point at 0 h p.i. for AC_p. Additionally, three of the following time points in hours post-injection were considered: 24, 48, 96, 144 and 192, which resulted in 10 time point combinations. The chosen values for rK_i were 1, 5 and 20 $\cdot 10^{-3}$ h^{-1}, representing real values of K_i for tissue without target expression [8], and two levels of target expression, respectively. The chosen rV_T were 0.1, 0.2 and 0.5. These values were comparable to baseline values for V_T as found by Jauw et al. [8], which agreed with predicted values for V_T as sum of antibody biodistribution coefficient [17] and the plasma volume fraction. The noise levels of the TAC at time 0 were varied from 5%, 10% to 15%, equal to noise levels for the TAC previously used in a Patlak simulation study [18]. Simulations were performed in MATLAB (v9.3.0.713579) [16] using in-house written code (see Additional file 1).

Results

Simulations showed that bias in K_i was negative in all situations, see Figs. 3, 4 and 5 and Table 2. Inclusion of a time point at 24 h p.i. improved accuracy and precision of Patlak results in almost all simulations. Simulations with

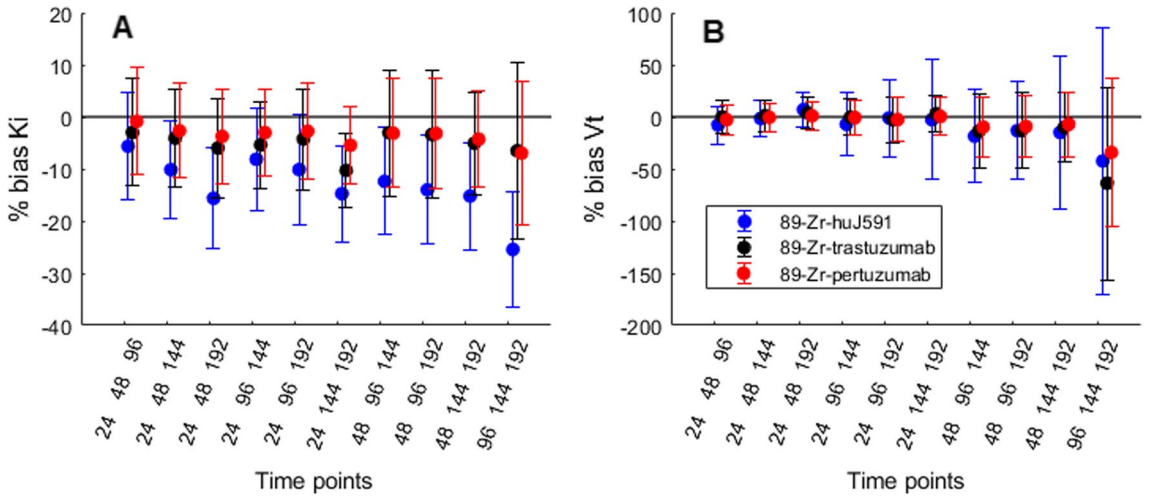

Fig. 3 Percentage bias and variability of K_i (**A**) and V_T (**B**) per time point combination, for ^{89}Zr-huJ591, ^{89}Zr-trastuzumab and ^{89}Zr-pertuzumab input functions and time activity curves with 5% noise, $rK_i = 5{\cdot}10^{-3}$ [h^{-1}] and $rV_T = 0.2$. Combinations including 24 h post-injection showed smaller bias and variability than combinations without 24 h p.i. rK_i = reference K_i, rV_T = reference V_T

^{89}Zr-huJ591, ^{89}Zr-trastuzumab and ^{89}Zr-pertuzumab IF, noise level of 5%, rK_i of $5{\cdot}10^{-3}$ h^{-1} and rV_T of 0.2 are shown in Fig. 3, and results are listed in Table 2. Including a time point at 24 h p.i. reduced bias and variability in V_T for all three IF. Bias in K_i was reduced for ^{89}Zr-huJ591 and remained similar for ^{89}Zr-trastuzumab and ^{89}Zr-pertuzumab. Variability in K_i remained similar for ^{89}Zr-huJ591 and reduced slightly for ^{89}Zr-trastuzumab and ^{89}Zr-pertuzumab. Therefore, time point 24 h p.i. was included in all subsequent simulations.

Simulations with ^{89}Zr-pertuzumab as IF and 5% noise level showed that bias in K_i ranged from −0.5% (absolute bias of $-5{\cdot}10^{-6}$ for $K_i = 1{\cdot}10^{-3}$ and $V_t = 0.1$) to −6% (absolute bias of $-1.1{\cdot}10^{-3}$ for $K_i = 20{\cdot}10^{-3}$ and $V_t = 0.5$) and bias in V_T ranged from 2% (absolute bias of 0.01 for $V_t = 0.5$ and $K_i = 1{\cdot}10^{-3}$) to −16% (absolute bias of −0.016 for $V_t = 0.1$ and $K_i = 1{\cdot}10^{-3}$). Increasing the values for rK_i and rV_T resulted in increased variability in K_i and V_T. Higher values for rK_i also increased bias in K_i. However, bias in K_i resulting from increased rV_T and bias in V_T resulting from increased rK_i and rV_T remained similar, see Fig. 4.

Simulations with ^{89}Zr-huJ591, ^{89}Zr-trastuzumab and ^{89}Zr-pertuzumab IF, rK_i of $1{\cdot}10^{-3}$ h^{-1} and rV_T of 0.2 showed a threefold increase in variability in K_i and V_T with higher noise levels, bias remained similar. For ^{89}Zr-huJ591, increasing the noise level from 5 to 15% increased variability in K_i (SE from 23.0 to 68.0% and from 30.0 to 90.6%, respectively) and variability in V_T (SE from 10.1 to 29.6% and 29.2 to 86.1%, respectively), while biases remained similar for K_i (from −4.9 to −5.1 and −16 to −16%, respectively) and V_T (from −1.6 to −2.3% and 2.3 to 1.8%, respectively). Results of the other two IFs showed the same pattern. The noise level dependency was similar for higher rK_i and rV_T, however with higher bias and variability because of increased rK_i and rV_T.

A decrease in AUC_p of the IF (in the order ^{89}Zr-pertuzumab, ^{89}Zr-trastuzumab, ^{89}Zr-huJ591) resulted in increased bias in K_i and increased variability in V_T with increased rK_i, see Fig. 5. For rK_i values of $20{\cdot}10^{-3}$ h^{-1}, bias in K_i also depended on the included time points, where the combinations 24, 48 and 192 h p.i. and 24, 144 and 192 h p.i. showed a larger underestimation of K_i of −16% (absolute bias of $-3.2{\cdot}10^{-3}$ for $K_i = 20{\cdot}10^{-3}$ and $V_t = 0.1$) for ^{89}Zr-huJ591 IF as compared to −10% for ^{89}Zr-trastuzumab (absolute bias of $-2.0{\cdot}10^{-3}$ for $K_i = 20{\cdot}10^{-3}$ and $V_t = 0.1$) and −5.4% for ^{89}Zr-pertuzumab IF (absolute bias of $-1.1{\cdot}10^{-3}$ for $K_i = 20{\cdot}10^{-3}$ and $V_t = 0.1$). Decreased AUC_p of the IF also showed increased variability in K_i and V_T for increased rV_T; however, bias remained similar.

Overall, when including time point 24 h p.i., there were only small differences found in bias and variability between different time point combinations. Only for high K_i values and the ^{89}Zr-huJ591 IF (with faster clearance of the ^{89}Zr-mAb from blood), bias in K_i and V_T showed a larger dependence on included time points, see Fig. 5. For all IFs, rK_i, rV_T, and time point combinations with noise level of 5%, percentage bias in K_i ranged from −0.5 to −16%.

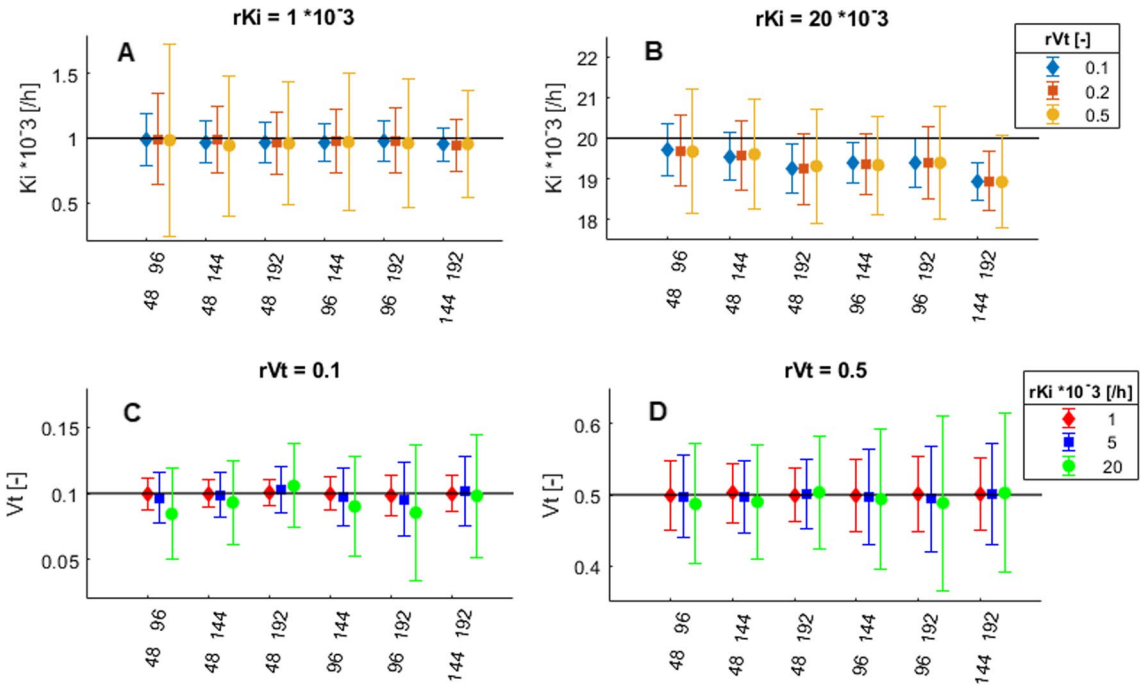

Fig. 4 Absolute K_i (**A** and **B**) and V_T (**C** and **D**) values per time point combination for $rK_i = 1$ and $20{\cdot}10^{-3}$ [h^{-1}], and for $rV_T = 0.1$ and 0.5, for ^{89}Zr-pertuzumab input function and time activity curves with 5% noise. All time point combinations on the x-axis also included 24 h post-injection. rK_i = reference K_i, rV_T = reference V_T

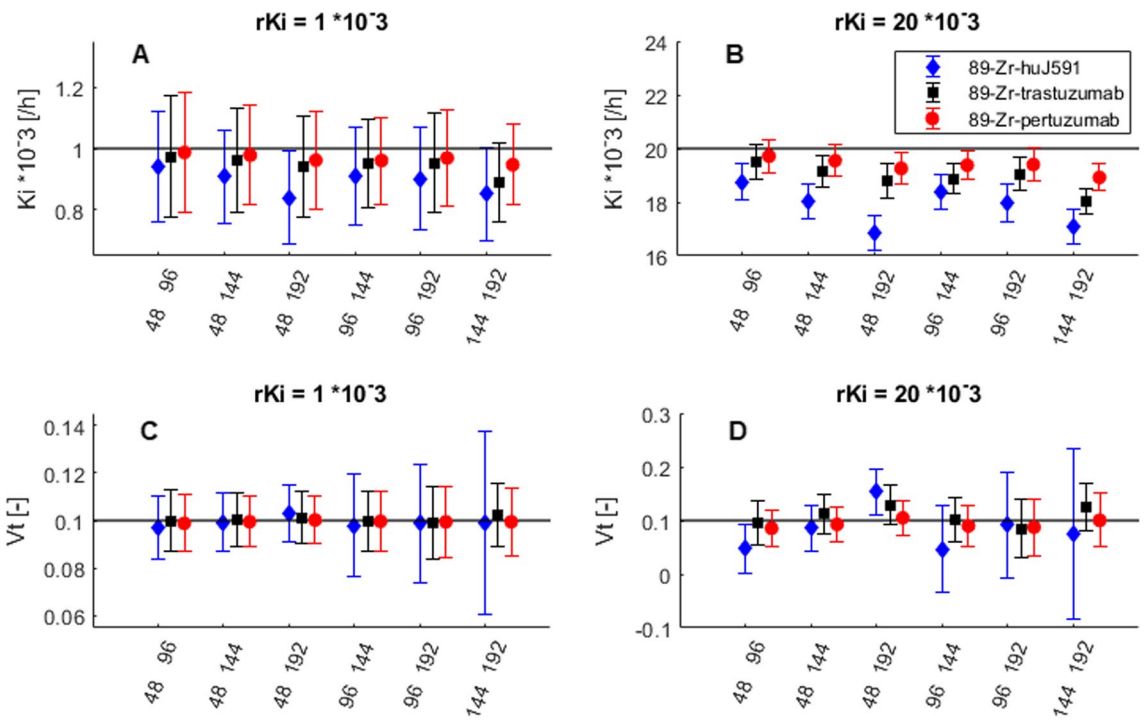

Fig. 5 Absolute K_i (**A** and **B**) and V_T (**C** and **D**) values per time point combination for ^{89}Zr-huJ591, ^{89}Zr-trastuzumab and ^{89}Zr-pertuzumab input functions, with $rK_i = 1$ and $20{\cdot}10^{-3}$ [h^{-1}], $rV_T = 0.1$ and time activity curves with 5% noise. All time point combinations on the x-axis also included 24 h post-injection. rK_i = reference K_i, rV_T = reference V_T

Table 2 Smallest and largest percentage bias and variability of simulations with and without time point 24 h p.i. for both K_i and V_T

	With 24 h		Without 24 h		With 24 h		Without 24 h	
	K_i				V_T			
	Smallest	Largest	Smallest	Largest	Smallest	Largest	Smallest	Largest
Bias (%)								
^{89}Zr-huJ591	−6.2	−16.2	−12.5	−24.9	−7.0	7.0	−9.3	−46.7
^{89}Zr-trastuzumab	−2.7	−10.0	−2.9	−8.1	−2.2	3.2	−11.2	−55.4
^{89}Zr-pertuzumab	−1.5	−5.0	−2.0	−6.4	−3.0	0.8	−8.4	−36.0
Variability (%)								
^{89}Zr-huJ591	9.2	11.1	9.9	10.9	16.3	57.4	43.6	127.6
^{89}Zr-trastuzumab	7.2	10.7	9.6	16.4	14.6	22.2	32.3	92.8
^{89}Zr-pertuzumab	7.4	10.5	9.1	13.9	13.2	20.5	28.3	71.6

Discussion

This study evaluated the effect of the choice of imaging time points on the accuracy and precision of Patlak linearization for ^{89}Zr-immuno-PET, considering different conditions. Simulations showed that inclusion of a PET scan and blood sample at 24 h p.i. improves accuracy and precision of Patlak results. Different combinations of later time points did not change the accuracy and precision in most cases. Moreover, increase in rK_i, rV_T and noise level decreased accuracy and precision of Patlak results. Additionally, IFs with smaller AUC_p showed decreased accuracy and precision of Patlak results as compared to IFs with larger AUC_p.

Underestimation of K_i

Bias in K_i was negative in all simulations. This can be explained by the shape of the IF in combination with the calculation of AUC_p in the Patlak equation [6]. In case the IF is fully described, for instance with a bi-exponential equation, determining the AUC_p by integration will result in the true value for AUC_p. However, when only a finite set of points is known from the IF, determining the AUC_p will be based on trapezoidal numerical integration. For the simulations in this study, the latter applies, because data sampling is always finite. Since the activity concentration in plasma decreases over time in an exponential manner, the shape of the IF is curved downwards, leading to an overestimation of the AUC_p with trapezoidal numerical integration. The overestimated AUC_p increases the x-coordinates of the Patlak plot, which is AUC_p/AC_p, while the y-coordinates remain the same, because the ratio AC_t/AC_p does not change. This results in a decreased positive slope of the Patlak plot, e.g., negative bias of K_i.

24 h time point

Inclusion of time point 24 h p.i. showed to improve accuracy and precision of Patlak linearization. This is also due to the better assessment of the shape of the IF and the calculation of AUC_p as detailed before. The better the curve of the IF is described, by adding a time point in the most curved part of the IF, the more accurate the determination of AUC_p and Patlak parameters. One assumption for Patlak linearization is that equilibrium is reached between the ^{89}Zr-mAb concentration in plasma and in the reversible tissue compartment, meaning that all fluxes are constant with respect to time [6]. In this study, activity concentrations in tissue were simulated by means of Patlak linearization and therefore were directly in equilibrium with activity concentrations in plasma. However, mAbs are relatively large proteins, therefore distribution inside the body takes relatively long, so tissue is not in rapid equilibrium with plasma [7]. Therapeutic antibodies cetuximab and trastuzumab showed approximately homogeneous distributions after 24 h p.i. in tumor-bearing mice [19]. For this reason, a period of 24 h was estimated to reach equilibrium between tissue and plasma. Additionally, from a practical point of view, it would not be possible to include time points after approximately 12 h, because PET scans should then be obtained outside working hours. Hence, time points before 24 h p.i. were not included in the simulations. This moment of equilibrium may differ between ^{89}Zr-mAbs, and inclusion of a slightly earlier or later time point may be better depending on the mAb pharmacokinetics.

Time point combinations

After inclusion of the 24 h p.i. time point, different time point combinations barely influenced Patlak results, which is advantageous from a practical perspective. Postponing a late imaging time point to a different day would not influence Patlak results. This is in contrast with obtaining the SUV, for which differences in the uptake time between injection and PET scan does influence the result, because SUV changes as a function of time [20]. In case the assumption of equal clearance between patients is true, comparisons of SUVs between patients

would only be possible for PET scans that are obtained at the same uptake time post-injection [4]. Therefore, postponing a PET scan, resulting in different scan days for patients accompanied by different plasma activity concentrations, will influence SUV results. Apart from the ability to distinguish between reversible and irreversible, and potentially between non-specific and specific uptake of ^{89}Zr-mAbs [8], the option to postpone a PET scan is another advantage of using Patlak linearization over using SUV in the quantification of ^{89}Zr-immuno-PET.

Reference K_i and V_T

Simulations showed that increasing rK_i and rV_T resulted in similar or increased bias and variability in both K_i and V_T. As Patlak linearization is only applied when the assumption of irreversible uptake is met, K_i is never zero. Additionally, Jauw et al. [8] showed that organs without target expression have K_i values higher than zero, representing the catabolic rate of ^{89}Zr-mAbs in healthy tissue. Values for K_i in this study are therefore all above zero.

Noise levels

In this study, noise was approximated based on counting statistics, which resulted in noise increasing over time. This was similar to results from a study about noise-induced variability in PET imaging for ^{89}Zr-immuno-PET, where recovery coefficients (RC) also increased over time from day 0 to day 6 [21]. RC was defined as 1.96*SD(%). RCs found for Kidney, lung, spleen and liver combined ranged from 2 to 11 [21], resulting in a maximum SD of approximately 5%. Similarly, SD derived from the RCs of tumor SUVpeak results in 15%. Simulations including TAC*s* with a 5% noise level may therefore represent biodistribution and TAC*s* with a 15% noise level may represent tumor uptake. Increasing the noise level from 5 to 15% only increased the variability, biases remained the same. Additionally, results of simulations with a noise level of 15% showed the same pattern as simulations with a 5% noise level and were chosen not to be presented.

Input functions

The literature search provided five different ^{89}Zr-mAb plasma IFs in patients, of which three were used for the simulations, while there are currently 119 therapeutic antibodies approved by the FDA [22]. However, these three ^{89}Zr-mAb plasma IFs used in this study provide a wide range of clearances, covering substantial variability in IFs.

Simulations showed a dependency of Patlak results on the IF. For high rK_i, accuracy and precision in Patlak results decreased with AUC of the IF (i.e., faster clearance), in the following order: ^{89}Zr-pertuzumab, ^{89}Zr-trastuzumab and ^{89}Zr-huJ591. A decrease in AUC_p will result in lower x-coordinates of the Patlak plot, thereby bringing the datapoints closer together resulting in higher contribution of noise. The AUC_p is the integral of the activity concentration in plasma, which is the total ^{89}Zr-mAbs present in the plasma cumulated over time from injection to moment of PET scan. For the simulations, the IF and rK_i were regarded as two independent variables; however, they are physiologically related. For IFs with lower AUC_p, so faster clearance, higher irreversible uptake in tissue (rK_i) is expected. However, simulations showed that a higher rK_i for the ^{89}Zr-huJ591 IF resulted in decreased accuracy of K_i (−16%) and precision of V_T as compared to the other IFs. This indicates that accuracy and precision of Patlak results are worse for ^{89}Zr-mAbs with faster clearance combined with higher irreversible uptake. However, for volumes of interest showing high irreversible uptake, a bias in K_i of −16% would not change the (clinical) decision-making based on the data, because the observed irreversible uptake would still be high.

This study considers input functions with binding of targets on cells that do not redistribute during the course of the PET studies (HER2 for trastuzumab and pertuzumab, and PSMA for huJ591). However, the usefulness of Patlak linearization may be limited in case of ^{89}Zr-mAbs that bind to mobile immune cells, such as the PD-1 receptors on T-cells. In order to apply Patlak linearization, an equilibrium between reversible processes is assumed as well as a constant density of specific targets or receptors. Changes in receptor availability during the course of the study may introduce inaccuracies in Patlak linearization. Yet, Patlak analysis also has several advantages over SUV. Patlak linearization can also be applied with higher mass dose. However, there are two phenomena that need to be considered. First of all, higher mass doses will result in slower plasma clearance. Patlak linearization takes into account the mAb concentration in plasma (or input function) and no assumptions are required with regard to (changes in) plasma clearance as the measured plasma kinetics are used. Secondly, a higher administered mass dose will result in lower uptake in tissue of interest. Patlak linearization is still valid with higher mass doses; however, lower K_i values are expected because of the reduced receptor availability/higher receptor or target occupancy. Also, Menke-van der Houven van Oordt et al. [9] showed in their study that Patlak linearization applied to PET imaging data with different administered mass doses allows evaluation of the optimal therapeutic dose. By plotting the Patlak K_i values against increasing mass doses a S-curve can be obtained. K_i values decrease because of target binding competition between labeled and unlabeled mAbs. This curve allows evaluation of the 50% inhibitory mass dose (ID50). The ID50, the dose at which 50% of the targets are occupied, can be used in establishing the optimal therapeutic dose [9].

Conclusion

This study evaluated the effect of imaging time points on the accuracy and precision of Patlak results, for different IFs, imaging time points, noise levels, and tissues with different levels of reversible and irreversible uptake. Quantification of ^{89}Zr-immuno-PET using Patlak linearization can generate accurate results within −0.5% and −16% bias for K_i (at a 5% noise level), provided that a 24 h p.i. time point and two later time points are included. The exact timing of the two other scans and samples is, however, not critical as opposed to SUV-based quantification.

Supplementary Information

The online version contains supplementary material available at https://doi.org/10.1186/s13550-022-00927-6.

Additional file 1. In-house written MATLAB code for Patlak linearization. The in-house written MATLAB function provided in Supplemental 1 was used for Patlak linearization calculations.

Acknowledgements
Not applicable

Author contributions
All authors contributed to the study conception and design. Data collection and analysis were performed by JW, MH and RB. The first draft of the manuscript was written by JW and all authors (MH, JP, WM, YJ and RB) commented on previous versions of the manuscript. All authors (JW, MH, JP, WM, YJ and RB) read and approved the final manuscript.

Funding
This work has received funding from the Innovative Medicines Initiative 2 Joint Undertaking (JU) under grant agreement No. 831514 (Immune-Image). The JU receives support from the European Union's Horizon 2020 research and innovation programme and EFPIA.

Availability of data and materials
All data and scripts generated during the current study are available from the corresponding author on reasonable request.

Declarations

Ethics approval and consent to participate
Not applicable.

Consent for publication
Not applicable.

Competing interests
The authors declare that they have no competing interests.

Author details
[1]Department of Radiology and Nuclear Medicine, Amsterdam UMC location Vrije Universiteit Amsterdam, Boelelaan 1117, Amsterdam, The Netherlands. [2]Department of Medical Oncology, Amsterdam UMC location Vrije Universiteit Amsterdam, Boelelaan 1117, Amsterdam, The Netherlands. [3]Department of Hematology, Amsterdam UMC location Vrije Universiteit Amsterdam, Boelelaan 1117, Amsterdam, The Netherlands. [4]Cancer Center Amsterdam, Imaging and Biomarkers, Amsterdam, The Netherlands.

Received: 10 January 2022 Accepted: 19 August 2022
Published online: 05 September 2022

References

1. Kimiz-Gebologlu I, Gulce-Iz S, Biray-Avci C. Monoclonal antibodies in cancer immunotherapy. Mol Biol Rep. 2018;45:2935–40.
2. van Dongen G, Beaino W, Windhorst AD, et al. The role of (89)Zr-immuno-PET in navigating and derisking the development of biopharmaceuticals. J Nucl Med. 2021;62:438–45.
3. Boellaard R. Standards for PET image acquisition and quantitative data analysis. J Nucl Med. 2009;50(Suppl 1):11S-20S.
4. Lammertsma AA, Hoekstra CJ, Giaccone G, Hoekstra OS. How should we analyse FDG PET studies for monitoring tumour response? Eur J Nucl Med Mol Imaging. 2006;33(Suppl 1):16–21.
5. Vriens D, Visser EP, de Geus-Oei LF, Oyen WJ. Methodological considerations in quantification of oncological FDG PET studies. Eur J Nucl Med Mol Imaging. 2010;37:1408–25.
6. Patlak CS, Blasberg RG, Fenstermacher JD. Graphical evaluation of blood-to-brain transfer constants from multiple-time uptake data. J Cereb Blood Flow Metab. 1983;3:1–7.
7. Lobo ED, Hansen RJ, Balthasar JP. Antibody pharmacokinetics and pharmacodynamics. J Pharm Sci. 2004;93:2645–68.
8. Jauw YWS, O'Donoghue JA, Zijlstra JM, et al. (89)Zr-Immuno-PET: toward a noninvasive clinical tool to measure target engagement of therapeutic antibodies in vivo. J Nucl Med. 2019;60:1825–32.
9. der Houven M, van Oordt CW, McGeoch A, Bergstrom M, et al. Immuno-PET imaging to assess target engagement: experience from (89)Zr-Anti-HER3 mAb (GSK2849330) in patients with solid tumors. J Nucl Med. 2019;60:902–9.
10. Pandit-Taskar N, O'Donoghue JA, Beylergil V, et al. (8)(9)Zr-huJ591 immuno-PET imaging in patients with advanced metastatic prostate cancer. Eur J Nucl Med Mol Imaging. 2014;41:2093–105.
11. O'Donoghue JA, Lewis JS, Pandit-Taskar N, et al. Pharmacokinetics, biodistribution, and radiation dosimetry for (89)Zr-trastuzumab in patients with esophagogastric cancer. J Nucl Med. 2018;59:161–6.
12. Ulaner GA, Lyashchenko SK, Riedl C, et al. First-in-human human epidermal growth factor receptor 2-targeted imaging using (89)Zr-Pertuzumab PET/CT: dosimetry and clinical application in patients with breast cancer. J Nucl Med. 2018;59:900–6.
13. O'Donoghue JA, Danila DC, Pandit-Taskar N, et al. Pharmacokinetics and biodistribution of a [(89)Zr]Zr-DFO-MSTP2109A anti-STEAP1 antibody in metastatic castration-resistant prostate cancer patients. Mol Pharm. 2019;16:3083–90.
14. Thorneloe KS, Sepp A, Zhang S, et al. The biodistribution and clearance of AlbudAb, a novel biopharmaceutical medicine platform, assessed via PET imaging in humans. EJNMMI Res. 2019;9:45.
15. Cherry SR, Sorenson J, Phelps ME, Methé BM. Physics in nuclear medicine. Med Phys. 2004;31:2370–1.
16. MATLAB. version 9.3.0.713579 (R2017b). Natick, Massachusetts: The MathWorks Inc.; 2017.
17. Shah DK, Betts AM. Antibody biodistribution coefficients: inferring tissue concentrations of monoclonal antibodies based on the plasma concentrations in several preclinical species and human. mAbs. 2013;5:297–305.
18. van Sluis J, Yaqub M, Brouwers AH, Dierckx R, Noordzij W, Boellaard R. Use of population input functions for reduced scan duration whole-body Patlak (18)F-FDG PET imaging. EJNMMI Phys. 2021;8:11.
19. Lee CM, Tannock IF. The distribution of the therapeutic monoclonal antibodies cetuximab and trastuzumab within solid tumors. BMC Cancer. 2010;10:255.
20. Keyes JW Jr. SUV: standard uptake or silly useless value? J Nucl Med. 1995;36:1836–9.
21. Jauw YWS, Heijtel DF, Zijlstra JM, et al. Noise-induced variability of immuno-PET with zirconium-89-labeled antibodies: an analysis based on count-reduced clinical images. Mol Imaging Biol. 2018;20:1025–34.
22. Cai HH. Therapeutic Monoclonal Antibodies Approved by FDA in 2020. Clin Res Immunol. 2021;4(1):1–2.

Publisher's Note